Mechanisms and kinetics of short pulse laser-induced destruction of silver-containing nanoparticles in multicomponent silicate photo-thermo-refractive glass

Julien Lumeau[1,2,*] and Leonid B. Glebov[2]

[1]Aix Marseille Université, CNRS, Centrale Marseille, Institut Fresnel UMR 7249, 13013 Marseille, France

[2]CREOL, The College of Optics and Photonics, University of Central Florida, P.O. Box 162700, Orlando, Florida 32816-2700, USA

*Corresponding author: julien.lumeau@fresnel.fr

Received 1 July 2014; revised 20 September 2014; accepted 20 September 2014; posted 23 September 2014 (Doc. ID 214506); published 27 October 2014

Photo-thermo-refractive (PTR) glass is a photosensitive multi-component silicate glass that is commercially used for the recording of volume holographic elements and finds many applications in advanced laser systems. Refractive index decrement in this glass is observed after UV exposure followed by thermal development. This procedure also causes the appearance of Ag-containing particles that can then be optically bleached by using the second harmonic of a Nd:YAG laser. Despite the broad usage of this method, its mechanisms are still unclear. In this paper, a systematic study of the short pulse laser-induced destruction of Ag-containing particles' kinetics versus incident energy per pulse and dosage is presented. We show that no bleaching of Ag-containing particles occurs for an energy density in laser pulses below 0.1 J/cm^2 while above 1 J/cm^2, the efficiency of bleaching saturates. Efficiency of bleaching depends on the type of particles to be bleached (Ag, AgBr…). Using a simple model of short pulse laser interaction with nanoparticles embedded in glass, the temperature of the Ag-containing particles reached during the laser interaction is shown to be large enough to produce complete dissipation of these particles which is expected to be the main mechanism of short pulse laser-induced destruction of Ag-containing particles.

OCIS codes: (160.5335) Photosensitive materials; (140.3538) Lasers, pulsed; (300.1030) Absorption.
http://dx.doi.org/10.1364/AO.53.007362

1. Introduction

Photo-thermo-refractive (PTR) glass is a sodium-potassium-zinc-aluminum-fluorine-bromine silicate glass doped with antimony, tin, cerium, and silver. This class of glasses, which undergo photo-thermo-induced crystallization, was invented by Stookey [1] many years ago and has been studied as a candidate for hologram writing in the last 20 years [2–5]. PTR glass exhibits a localized refractive index decrement after UV exposure and successive thermal treatment above the glass transition temperature, Tg, which results from the crystallization of about 0.5 wt. % sodium fluoride nanocrystals [6]. The possibility of recording phase holograms in this glass has the potential for many high tech applications, such as optical filtering [7] and spectral beam combining of high power lasers [8].

A description of the complex photo-thermo-induced crystallization mechanisms in this type of glass is given in Ref. [9]. The evolution of the material's nanostructure and optical properties after UV-exposure and thermal treatment are reported in

1559-128X/14/317362-07$15.00/0

several publications, e.g., [6,10–14]. Actually, it was shown in Ref. [6] that the photosensitivity of PTR glass results from the precipitation of nanosized sodium fluoride crystals within the glass matrix in the UV-exposed regions after heat treatment. A simplified mechanism for photothermal crystallization is the following: before any thermal development of the glass, sodium, fluorine, and all other ions are uniformly dissolved in the matrix and the material is totally vitreous. When PTR glass is exposed to long wavelength UV radiation $\lambda > 250$ nm (e.g., He–Cd laser at 325 nm), Ce^{3+} releases an electron and converts to a hole-type Ce^{4+} center. The released electron is then trapped by intrinsic defects of the glass matrix or dopants and impurities in the highest valence state, including silver ions dispersed in the glass matrix. Then, silver ions convert to silver atoms. When a UV-exposed glass is nucleated at temperatures between 450 and 500°C, silver atoms agglomerate and form colloidal silver particles. It was also demonstrated that silver bromide clusters form [15]. The second part of the crystallization process consists of the heterogeneous precipitation and growth of sodium fluoride crystals on top of the silver (or silver bromide) clusters. NaF growth is then controlled by the diffusion of sodium and fluorine from the glass matrix to the crystals [14]. It is seen that the presence of Ag-containing particles is a mandatory step in the photo-induced crystallization. Moreover, it is very well known that the appearance of silver colloidal particles will induce a plasmon resonance that will result in an induced absorption band whose position and width will depend on their composition and diameter. In Refs. [15,16] it was shown that, depending on the size distribution and on the presence of halides (bromine or chlorine, for example), the position of the induced absorption band may vary from 400 to 600 nm. Typical losses spectrum of UV-exposed (4 J/cm^2 at 325 nm) and thermally developed (1 h at 515°C) PTR glass in the range from 300 to 1500 nm is shown in Fig. 1. There are several sources that contribute to the losses of PTR glass. In the UV region, there is the superposition of the absorption of cerium +III, the induced absorption of silver-containing particles, and the scattering while at longer wavelengths, the main contributions are from the induced absorption of silver-containing particles and the scattering. Moreover, it was shown in Ref. [17], that this band can be fully optically bleached using the second harmonic of a Nd:YAG laser at 532 nm (Fig. 1).

Using this technique it becomes possible to extract the induced absorption band of the silver-containing particles by subtracting the losses spectra before and after this optical bleaching. Fig. 2 [16] shows a typical induced absorption spectrum of silver-containing particles. This band is centered at ~22000 cm^{-1}; i.e., ~465 nm and extends from 300 to 1500 nm.

Despite this well-known phenomenon of bleaching, the kinetics of this effect, as well as its mechanisms, are unclear. In this paper we investigate the kinetics of short pulse laser-induced destruction of Ag-containing particles as well as the ranges of intensities that are required for getting an efficient bleaching. Then, the evolution of the absorption spectra in the process of bleaching is analyzed. Finally, by analogy with the effects that were observed in a solution with metallic nanoparticle suspensions, a model for explaining the observed effects is proposed.

2. Experimental and sample preparation

A. PTR Glass Preparation

Samples of a photosensitive PTR glass containing $15Na_2O$-$5ZnO$-$4Al_2O_3$-$70SiO_2$-$5NaF$-$1KBr$-$0.01Ag_2O$-$0.01CeO_2$ (mol. %) and minor amounts of Sn and Sb were used in this work, as in previous studies [6,10–12]. Polished 25 mm × 25 mm × 5 mm samples were prepared from the batch. The chemical homogeneity of the samples is a critical parameter affecting crystallization properties [18], thus homogeneity was tested by the shadow method in a divergent beam of a He–Ne laser and was quantified by measurements using an interferometer (GPI Zygo). The samples selected for this study had refractive index fluctuations of less than 40 ppm (peak-to-valley) across the aperture.

B. UV-Exposure and Heat-Treatments

UV-exposure of samples was performed by a He–Cd laser (4 mW, 325 nm). Samples were homogeneously

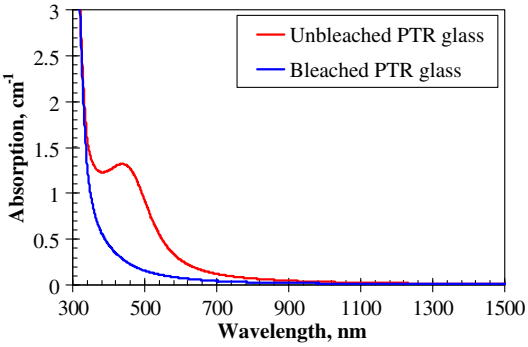

Fig. 1. Absorption spectra of UV-exposed and thermally developped PTR glass before and after optical beaching using the second harmonic of a Nd:YAG laser.

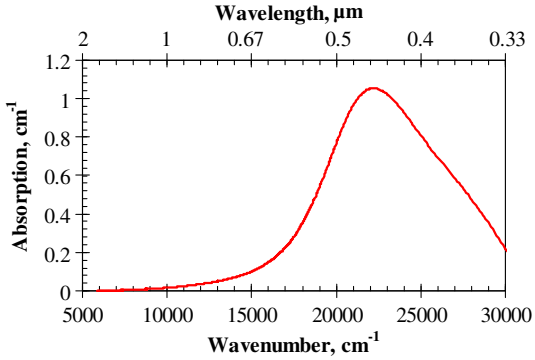

Fig. 2. Induced absorption spectrum of the silver-containing particles in PTR glass obtained by subtraction of the spectra of Fig. 1 [16].

exposed to a dosage of 4 J/cm^2 by scanning several overlapped lines on the sample. The dosage was controlled with the scanning speed [10]. This dosage was chosen in order to induce an absorption band of the silver-containing particles with amplitude large enough to allow its accurate measurement using a conventional dual beam spectrophotometer. The samples were then heat treated at 480°C and/or 515°C. The samples heat treated at 480°C were dropped inside a hot furnace and then quenched at the end of each thermal treatment in order to control the thermal treatment duration with a precision better than 1 min and to allow performing short thermal treatments. Samples heat treated at 515°C were heated from room temperature to 515°C at a rate of about 20 K/min and then cooled down to room temperature in the furnace following the natural decrease of the furnace temperature (about 2.5 K/min). Finally, in order to remove any incipient crystallization on the surfaces, each sample was ground and repolished with a flatness better than $\lambda/2$ at 633 nm.

C. Spectra Measurements

Transmission spectra were measured using a Perkin Elmer Lambda 950 spectrophotometer in the range from 200 to 1700 nm. Then, the spectral dependence of the losses coefficient was calculated by subtracting from the transmission spectra the reflection spectrum of the PTR glass that was calculated from the measured refractive index dispersion curve [19]. The absolute precision of such spectrophotometric measurement is limited to about $2 \cdot 10^{-2}$ cm^{-1}; i.e., about one order of magnitude larger than its relative precision. Each curve was thus calibrated. To achieve a precise measurement of the transmission the reflection at 1085 nm was carried out on each sample by photometric measurement using an Yb fiber laser. Then, losses were calculated at this wavelength, with precision of 10^{-3} cm^{-1}, and all spectra were stitched to the measured value of losses at 1085 nm. Using this technique, the absolute precision of each spectrum was improved to 10^{-3} cm^{-1}.

3. Kinetics of Short Pulse Laser-Induced Destruction of Ag-Containing Particles in UV-Exposed and Thermally Developed PTR Glass

A. Evolution of the Transmission at 532 nm in the Process of Bleaching

The simplest method that can be implemented for studying the efficiency of bleaching consists of measuring the evolution of the light coming from the second harmonic of a Nd:YAG laser and transmitted through the glass sample being bleached as a function of the dosage of bleaching. The setup used to perform this measurement is shown in Fig. 3.

The beam from the second harmonic of a Continuum Minilite Nd:YAG laser at 532 nm was focused with a 200 mm lens and the sample to be bleached was placed after the focal plane of the lens such that the beam diameter was equal to 1 mm at $1/e^2$. After

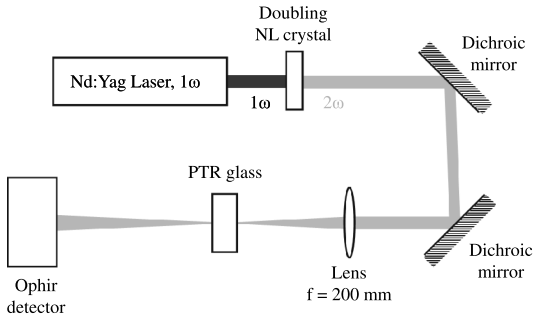

Fig. 3. Scheme of the setup used for studying the kinetics and mechanisms of optical bleaching of silver-containing particles in PTR glass.

the sample, an Ophir detector was added in order to measure the evolution of the transmitted energy as a function of time. The energy per pulse was varied from 0.36 to 2.15 J/cm^2. The pulse duration was equal to ~7 ns and the repetition rate was equal to 15 Hz. Using these parameters, the beam intensity and dosage were recalculated. Dosages from 100 to 800 J/cm^2 were used. Figure 4 shows the evolution of the transmission versus dosage for different energy per pulse in a PTR glass sample that was UV-exposed with a dosage of 4 J/cm^2, nucleated for 100 min at 485°C and finally thermally developed for 1 h at 515°C.

It is seen that the higher the energy per pulse, the steeper the slope at zero dosage. It is also seen that at an energy per pulse exceeding 1 J/cm^2, the slope at zero dosage tends to saturate and all curves tend to overlap. In order to quantify these findings, each curve of the dependence of the transmission $[T(D)]$ on dosage (D) was fitted with hyperbolic functions with the form

$$T(D) = \frac{\alpha D}{D + k}, \tag{1}$$

where α is the transmission after complete bleaching. Due to the level of scattering at 532 nm, the final transmission after complete bleaching was equal to 86%, meaning that the value of α was fixed to 0.86 (Fig. 5). The only remaining fitting parameter was the parameter, k, characteristic of the bleaching

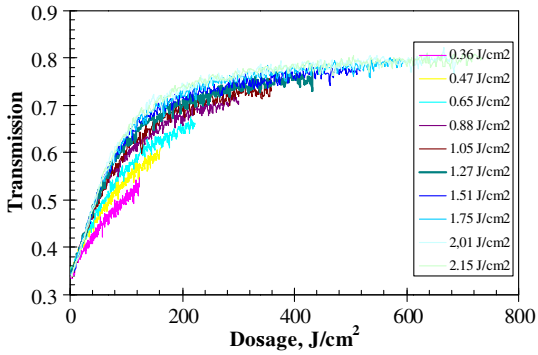

Fig. 4. Evolution of the Nd:YAG laser power transmitted through the PTR glass being bleached as a function of the dosage of exposure for different incident energies per pulse.

efficiency; the smaller the value of k, the higher the efficiency.

Finally, the dependence of the parameter, k, on the energy per pulse was plotted in Fig. 6. The parameter, k, decreases quickly when the energy per pulse is lower than 1 J/cm^2 and then tends to saturate when the energy per pulse exceeds 1 J/cm^2. No data were taken above 2 J/cm^2, as the probability of surface or bulk damage where platinum inclusions can be found increases. Such energy per pulse dependence reflects a nonlinear process, but cannot be associated with any multiphoton absorption process as increasing the energy per pulse should result in an increase of the bleaching efficiency.

B. Evolution of the Losses Spectra in the Process of Bleaching

In order to gain some insights on the mechanisms of bleaching, the evolution of the losses spectra was measured in the process of bleaching. The same exposure station at 532 nm as the one in Fig. 3 was used to perform the bleaching. PTR glass samples similar to the one used in the 532 nm transmission experiment were used for this experiment, i.e., samples were UV-exposed with a dosage of 4 J/cm^2, nucleated, and finally thermally developed for 1 h at 515°C. Dosage was increased by increasing the number of 532 nm pulses going through the PTR glass sample and spectra were measured after 532 nm exposure at different dosages and for different energy density per pulse. In order to study the kinetics of the silver-containing particles' disappearance, the bleaching efficiency $[\eta(\mathrm{BL}=i)]$ was then calculated after a number of bleachings (BL) equal to i using Eq. (2),

$$\eta(\mathrm{BL}=i)=1-\frac{\underset{\lambda}{\mathrm{Max}}[L(\lambda,\mathrm{BL}=i)-L(\lambda,\mathrm{BL}=N)]}{\underset{\lambda}{\mathrm{Max}}[L(\lambda,\mathrm{BL}=0)-L(\lambda,\mathrm{BL}=N)]}, \tag{2}$$

where $L(\lambda,\mathrm{BL}=i)$ is the evolution of the losses coefficient in the range [400–500] nm after a number of bleachings equal to i, $L(\lambda,\mathrm{BL}=0)$ is the evolution of the losses coefficient in the range [400–500] nm before bleaching and $L(\lambda,\mathrm{BL}=N)$ is the evolution of the losses coefficient in the range [400–500] nm after complete bleaching. Max represents the maximum of the function between the brackets. The typical evolution of the bleaching efficiency versus the 532 nm dosage for 1.05 J/cm^2 is shown in Fig. 7.

Similar measurements were carried out in samples exposed with different energy per pulse at 532 nm and then each curve was fitted with a hyperbolic function similar to the one in Eq. (1) but with α equal to 1. Figure 8 shows the dependence of the k parameter on the energy per pulse. As expected, Fig. 8 exhibits a similar behavior as the one that was observed in Fig. 6, meaning that the features that were seen at a single wavelength are valid for the whole spectrum of silver-containing particles' absorption band and that saturation of the bleaching efficiency above 1 J/cm^2 is not a spectrally localized feature, but an overall one.

C. Kinetics of Optical Spectra in UV-Exposed and Thermally Developed PTR Glass

It was seen in the previous sections that bleaching of the silver-containing particles is an overall effect that results in a decrease of the whole silver-containing particles' absorption band, but until now the specific properties of this effect, such as possible distortions of the shape of the spectra during the process of bleaching of UV-exposed and thermally developed PTR glass were not studied. UV-exposed and nucleated samples

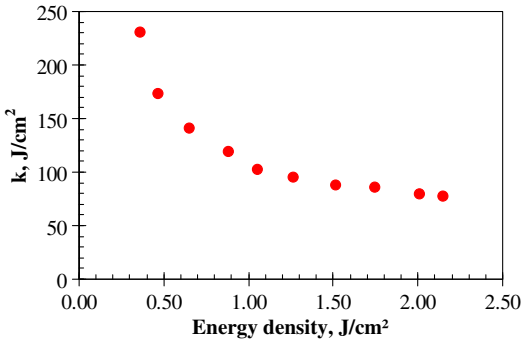

Fig. 6. Evolution of the k parameter of the hyperbolic function used to fit the curves of Fig. 4.

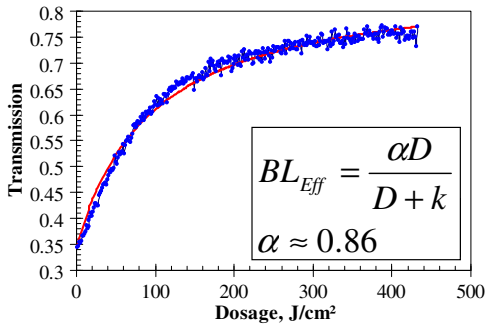

Fig. 5. Evolution of the Nd:YAG laser power transmitted through the PTR glass being bleached as a function of the dosage of exposure for an energy per pulse of 1.05 J/cm^2 and its fit using a hyperbolic function.

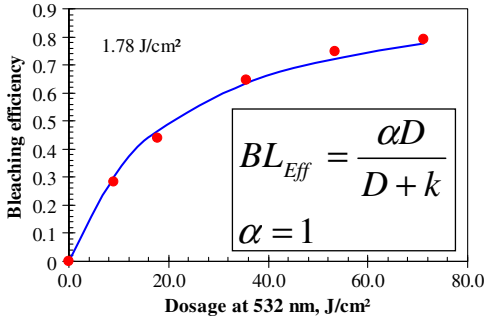

Fig. 7. Evolution of the amplitude at maximum of the silver-containing particles' induced absorption band that was bleached using the second harmonic of a Nd:YAG laser with an energy per pulse of 1.05 J/cm^2 and its fit using a hyperbolic function.

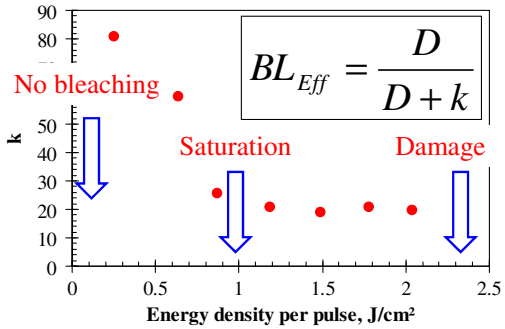

Fig. 8. Evolution of the k parameter of the hyperbolic function used to fit the curves similar to Fig. 7 and obtained for different energy per pulse.

(not heat treated to promote crystal growth) were used to perform this study. These samples are very attractive because they do not present any significant scattering and because they can show very specific features. It was shown in Refs. [15,16] that the structure of the silver-containing particles evolves significantly during the process of nucleation. It was also shown that the spectra of silver-containing particles can be perfectly fitted using 4 Gaussian bands, two of them presenting a long wavelength exponential Urbach tail. Parameters of these bands are summarized in Tables 1 and 2. Each band was associated with a different kind of particle, i.e., hole center, silver particle, silver bromide particle, and a complex silver bromide particle tentatively associated with a silver bromide particle surrounded with a silver shell. Using these as decomposition, it was demonstrated that the structure of the silver-containing particles' absorption band of samples nucleated for 5 min at 485°C is the superposition of the bands of hole centers, silver and silver bromide particles, all bands having almost the same amplitude, while the structure of the silver-containing particles' absorption band of samples nucleated for 100 min at 485°C is composed of the bands of hole centers, silver bromide particles, and silver bromide particles with silver shell, the first and third having similar amplitudes and the second one having twice the amplitude. Using such samples, it becomes possible to separate the kinetics of the bleaching of each particle as well as to reveal some aspects of the bleaching mechanisms.

PTR glass samples were exposed at 325 nm with a dosage of 4/cm^2 and nucleated for 5 and 100 min at 485°C. Samples were bleached using the second harmonic of a Nd:YAG laser and the bleaching dosage was linearly increased from 1 to 60 a.u. in the samples

Table 1. Parameters of the Gaussian Bands Used for Decomposing the Silver-Containing Induced Absorption Band in PTR Glass

	G4	G3	G2	G1
σ_i^0	26575	24275	22000	19500
$\Delta\sigma i$	3465	2055	3200	2800
λ_i^0	376	412	455	613
Origin	Hole	Ag	AgBr	Ag/AgBr

Table 2. Parameters of the Exponential Tails Used for Decomposing the Silver-Containing Induced Absorption Band in PTR Glass

	G4	G3
α_i	8	7.2
σi	20040	18051
$\alpha_i/\sigma i$	4×10^{-4}	4×10^{-4}

nucleated for 5 min at 485°C while the dosage was increased from 1 to 30 a.u. in the samples nucleated for 100 min at 485°C. However, the exact definition of the bleaching dosage could not be obtained, due to the fact that in order to increase the measurement aperture and the precision of the measurement, the sample was scanned within the beam of the 532 nm laser with a speed of 2 mm/s and an energy per pulse of 1 J/cm^2. However, the relative increase of the dosage could be obtained due to the fact that the bleaching procedure was kept constant throughout the experiment. Spectra were measured after some given dosages (Figs. 9 and 10). In the case of the samples nucleated for 5 min at 485°C, one can see that the maximum of the band of silver-containing particles tends to shift toward larger wavelengths during the beginning of the bleaching process and then tends to shift back.

Further analysis was obtained by applying a similar strategy as the one presented in Refs. [15,16]. Each induced absorption spectrum of silver-containing particles was decomposed into the sum of Gaussian functions with a precision of a few percent using the model of Refs. [15,16] and the evolution of the amplitude of each band was plotted as a function of dosage (Figs. 11 and 12). The extracted amplitude of each of the silver-containing particles is nonmonotonously decreasing when the dosage increases. More precisely, the observed evolution of each of the silver-containing particles' absorption band is similar to the one that was shown in the process of nucleation of PTR glass [15,16]. Therefore, while the main effect of the bleaching is an overall decrease of the volume fraction of the silver-containing particles and, therefore, a decrease of the overall induced absorption band, additional

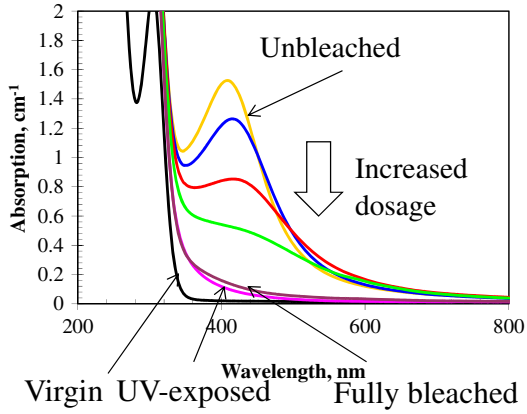

Fig. 9. Evolution of the absorption spectra of a sample nucleated for 5 min at 485°C in the process of bleaching.

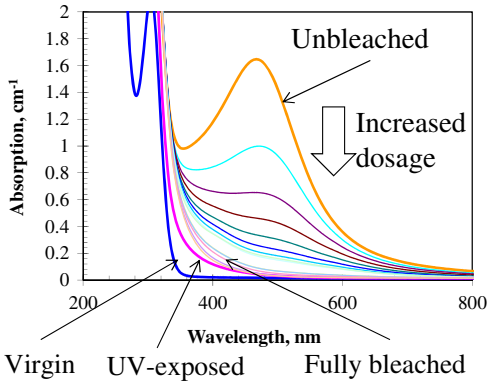

Fig. 10. Evolution of the absorption spectra of a sample nucleated for 100 min at 485°C in the process of bleaching.

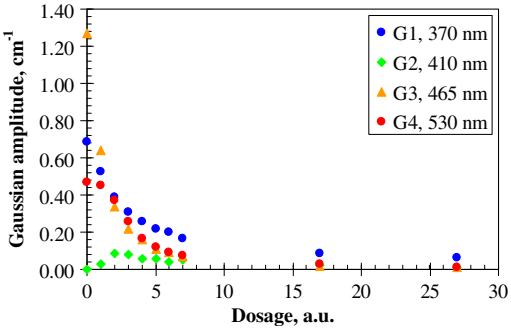

Fig. 12. Evolution of the amplitude of each of the 4 Gaussian bands used to fit the absorption spectra of a sample nucleated for 100 min at 485°C in the process of bleaching as shown in Fig. 10.

effects appear in parallel, such as the appearance of new particles.

D. Analysis of the Possible Mechanisms of Bleaching of Silver-Containing Particles

The destruction of metallic nanoparticles has already been studied in the past. There are numerous publications describing the mechanisms of bleaching of silver nanoparticles, their photodestruction, photofragmentation, and photoionization when they are dispersed in liquids [20–27]. It was demonstrated that using nanosecond or femtosecond lasers, it is possible to evaporate the particles so that they are completely dissipated inside the liquid or to change their size or shape and consequently their associated plasmon resonance properties. Similar efficiency curves were also measured [22]. In addition, the destruction of metallic nanoparticles in glass by short pulse laser was thoroughly studied by the laser damage community 10 years ago as the presence of metallic nanoparticles, such as platinum, was shown to be one of the causes of laser damage in optical glasses. In one of these studies [28] a simple model of such effect was developed and applied to nanoparticles of gold dispersed in a glass matrix. It was shown that the energy absorbed by one particle is

$$E_p = F\pi R^2, \tag{3}$$

while the energy for vaporization of one particle is

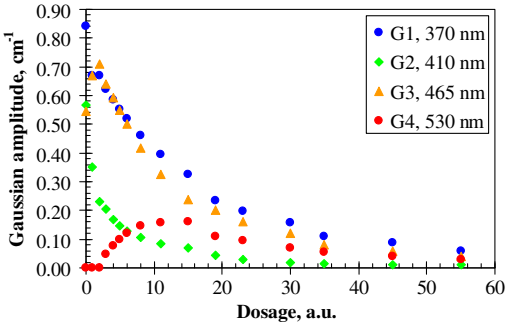

Fig. 11. Evolution of the amplitude of each of the 4 Gaussian bands used to fit the absorption spectra of a sample nucleated for 5 min at 485°C in the process of bleaching shown in Fig. 9.

$$E_{\mathrm{cr}} = C\rho V(T_{\mathrm{boiling}} - 293K) + (H_{\mathrm{fusion}} + H_{\mathrm{vap}})V. \tag{4}$$

Using induced absorption spectra of silver-containing particles it is possible to estimate an approximate value of the average size of silver particles, $\langle d\rangle$,

$$\langle d\rangle = \frac{v_F}{2\pi c} \times \frac{\lambda^2}{\Delta\lambda}. \tag{5}$$

By evaluating the wavelength of the maximum absorption peak (λ) and its FWHM ($\Delta\lambda$), v_F being the Fermi velocity of electrons in bulk metal (silver $= 1.39 \times 108$ cm/s), it is possible to calculate the size of silver-containing particles (Table 3).

Using this theory, $\langle d\rangle$ was estimated to be ~20 angstroms. Using this value, the average energy absorbed by a 1 nm radius particle illuminated by a 1 J/cm^2 beam is equal to $\sim 1.3 \times 10^{-15}$ J. The energy required for vaporizing silver particles is equal to $\sim 2.5 \times 10^{-16}$ J and the energy required for vaporizing silver bromide particles is equal to $\sim 7 \times 10^{-17}$ J. These data demonstrate that the average absorbed energy is several times larger than that required for vaporizing any Ag-containing particles in PTR glass and that bleaching is a thermo-optical process. One must, however, keep in mind that the huge increase of temperature happens in the particle, but not in the surrounding glass so that it appears to have a very large gradient of temperature at the interface between the particle and the glass. Absorption of the pulse occurs during a few nanoseconds. Then, a very fast cooling of the particle occurs due to the diffusion of the heat toward the cold glass matrix that prevents the particle from being destroyed in one pulse. These data demonstrate that bleaching is not a pure optical effect but a

Table 3. Calculation of the Average Radius of the Silver-Containing Particles Based on the Plasmon Resonance Theory

Element	λ, nm	$\Delta\lambda$, nm	$\langle r\rangle$, m
σ_i^0	412	58	2.2×10^{-9}
$\Delta\sigma i$	454	111	1.4×10^{-9}
λ_i^0	513	124	1.6×10^{-9}

thermo-optical process, which also explains the evolution that was observed in Figs. 9–12. Actually, the very high amount of energy associated with the absorption of the pulse by the particles results in an increase of the local temperature of the particle that is analogous to a conventional heat treatment in an electrical furnace and that allows a thermal modification of the particles, analogous to that observed in the process of nucleation in PTR glass [15,16]. The bleaching process is therefore a thermo-optical process which consists in two concurrent processes happening during the pulse duration and a short duration after: while outer part of the silver containing particles can diffuse through the glass matrix and produce a partial destruction of the particles, the inner part of the particles has enough energy to produce a conversion of the particles similar to the one observed during the process of bleaching.

4. Conclusion

Kinetics and mechanisms of bleaching of the absorption band of silver-containing particles by the second harmonic of a Nd:YAG laser was studied. The process of bleaching is a nonlinear process as it occurs above an energy density threshold estimated to be around $\sim 0.1\ J/cm^2$. Efficiency of bleaching is increasing and then saturates when energy density reaches $\sim 1\ J/cm^2$ until reaching damage. Optical bleaching of silver-containing nanoparticles is a thermo-optical process based on the gradual dissipation of these particles as the number of pulses is increased. Finally, temperature increase during the process of bleaching has a similar impact as heating up the PTR glass to high temperature, i.e., it is continuing the process of nucleation of the silver-containing particles.

The authors want to thank Larissa Glebova for providing PTR glass, Karima Chamma for preparing the PTR glass samples and Vadim Smirnov for the very fruitful discussions.

References

1. S. D. Stookey, "Photosensitive glass—a new photographic medium," Ind. Eng. Chem. **41**, 856–861 (1949).
2. V. A. Borgman, L. B. Glebov, N. V. Nikonorov, G. T. Petrovskii, V. V. Savvin, and A. D. Tsvetkov, "Photo-thermal refractive effect in silicate glasses," Sov. Phys. Dokl. **34**, 1011–1013 (1989).
3. O. M. Efimov, L. B. Glebov, L. N. Glebova, K. C. Richardson, and V. I. Smirnov, "High-efficiency Bragg gratings in photothermorefractive glass," Appl. Opt. **38**, 619–627 (1999).
4. O. M. Efimov, L. B. Glebov, S. Papernov, and A. W. Schmid, "Laser-induced damage of photo-thermo-refractive glasses for optical-holographic-element writing," Proc. SPIE **3578**, 554–575 (1999).
5. O. M. Efimov, L. B. Glebov, and V. I. Smirnov, "High-frequency Bragg gratings in a photothermorefractive glass," Opt. Lett. **25**, 1693–1695 (2000).
6. T. Cardinal, O. M. Efimov, H. G. Francois-Saint-Cyr, L. B. Glebov, L. N. Glebova, and V. I. Smirnov, "Comparative study of photo-induced variations of X-ray diffraction and refractive index in photo-thermo-refractive glass," J. Non-Cryst. Solids **325**, 275–281 (2003).
7. L. B. Glebov, V. I. Smirnov, C. M. Stickley, and I. V. Ciapurin, "New approach to robust optics for HEL systems," Proc. SPIE **4724**, 101–109 (2002).
8. L. B. Glebov, "Photosensitive holographic glass—new approach to creation of high power lasers," Phys. Chem. Glasses **48**, 123–128 (2007).
9. D. Stookey, G. H. Beall, and J. E. Pierson, "Full-color photosensitive glass," J. Appl. Phys. **49**, 5114–5213 (1978).
10. O. M. Efimov, L. B. Glebov, and H. P. Andre, "Measurement of the induced refractive index in a photothermorefractive glass by a liquid-cell shearing interferometer," Appl. Opt. **41**, 1864–1871 (2002).
11. L. B. Glebov and L. Glebova, "Swelling of photo-thermo-refractive glass resulted from thermal development," Glass Sci. Technol. **75 C2**, 294–297 (2002).
12. L. Glebov, L. Glebova, V. Tsechomskii, and V. Golubkov, "Study of structural transformations in photo-thermo-refractive glass by SAXS and XRD," *Proceedings of XX International Congress on Glass*, Kyoto, Japan, September 2004.
13. M. Hass, J. W. Davisson, H. B. Rosenstock, and J. Babiskin, "Measurement of very low absorption coefficients by laser calorimetry," Appl. Opt. **14**, 1128–1130 (1975).
14. L. B. Glebov, "Volume hologram recording in inorganic glasses," Glass Sci. Technol. **75 C1**, 73–90 (2002).
15. J. Lumeau, L. Glebova, and L. B. Glebov, "Evolution of absorption spectra in the process of nucleation in photo-ihermo-refractive glass," Adv. Mater. Res. **39–40**, 395–398 (2008).
16. J. Lumeau, L. Glebova, and L. Glebov, "Absorption and scattering in photo-thermo-refractive glass induced by UV exposure and thermal development," Opt. Mater. **36**, 621–627 (2014).
17. L. B. Glebov and V. I. Smirnov, "Interaction of photo-thermo-refractive glass with nanosecond pulses at 532 nm," Proc. SPIE **5273**, 396–401 (2004).
18. J. Lumeau, A. Sinitskiy, L. N. Glebova, L. B. Glebov, and E. D. Zanotto, "Method to assess the homogeneity of photosensitive glasses: application to photo-thermo-refractive glass," J. Non Cryst. Solids **355**, 1760–1768 (2009).
19. J. Lumeau and L. B. Glebov, "Refractive index measurements in photo-thermo-refractive glass at different stages of hologram fabrication," *8th Pacific Rim Conference on Ceramic and Glass Technology (PACRIM 8)*, Vancouver, British Columbia, Canada, June, 2009), paper PACRIM8-S25-P205-2009.
20. H. Kurita, A. Takami, and S. Kodaa, "Size reduction of gold particles in aqueous solution by pulsed laser irradiation," Appl. Phys. Lett. **72**, 789–791 (1998).
21. S. Link, C. Burda, M. B. Mohamed, B. Nikoobakht, and M. A. El-Sayed, "Laser photothermal melting and fragmentation of gold nanorods: energy and laser pulse-width dependence," J. Phys. Chem. A **103**, 1165–1170 (1999).
22. A. Takami, H. Kurita, and S. Koda, "Laser-induced size reduction of noble metal particles," J. Phys. Chem. B **103**, 1226–1232 (1999).
23. T. Tsuji, N. Watanabe, and M. Tsuji, "Laser induced morphology change of silver colloids: formation of nano-size wires," Appl. Surf. Sci. **211**, 189–193 (2003).
24. R. Jin, Y. W. Cao, C. A. Mirkin, K. L. Kelly, G. C. Schatz, and J. G. Zheng, "Photoinduced conversion of silver nanospheres to nanoprisms," Science **294**, 1901–1903 (2001).
25. S. Eustis, G. Krylova, A. Eremenko, N. Smirnova, A. W. Schill, and M. El-Sayed, "Growth and fragmentation of silver nanoparticles in their synthesis with a fs laser and CW light by photo-sensitization with benzophenone," Photochem. Photobiol. Sci. **4**, 154–159 (2005).
26. Y. Badr, M. G. Abd El Wahed, and M. A. Mahmoud, "On 308 nm photofragmentation of the silver nanoparticles," Appl. Surf. Sci. **253**, 2502–2507 (2006).
27. P. V. Kamat, M. Flumiani, and G. V. Hartland, "Picosecond dynamics of silver nanoclusters. photoejection of electrons and fragmentation," J. Phys. Chem. B **102**, 3123–3128 (1998).
28. S. Papernova and A. W. Schmid, "Correlations between embedded single gold nanoparticles in SiO_2 thin film and nanoscale crater formation induced by pulsed-laser radiation," J. Appl. Phys. **92**, 5720–5728 (2002).